Composites Science and Technology 69 (2009) 2178–2184

Contents lists available at ScienceDirect

Composites Science and Technology

journal homepage: www.elsevier.com/locate/compscitech

TriSilanolPhenyl POSS–polyimide nanocomposites: Structure–properties relationship

R. Verker [a,b,*], E. Grossman [a], I. Gouzman [a], N. Eliaz [b]

[a] Space Environment Section, Soreq NRC, Yavne 81800, Israel
[b] School of Mechanical Engineering, Tel-Aviv University, Ramat Aviv, Tel-Aviv 69978, Israel

ARTICLE INFO

Article history:
Received 2 December 2008
Received in revised form 26 May 2009
Accepted 2 June 2009
Available online 7 June 2009

Keywords:
A. Nanocomposites
B. Fracture
B. Mechanical properties
D. Atomic force microscopy (AFM)
POSS–polyimide

ABSTRACT

Polyhedral Oligomeric Silsesquioxane (POSS)–polyimide (PI) thin films were synthesized from pre-mixed solution of oxydianiline–pyromellitic dianhydryde (ODA–PMDA) and TriSilanolPhenyl (TSP) POSS. POSS–PI polymerization reaction kinetics was studied using Fourier Transform Infrared (FTIR) spectroscopy. The POSS–PI films were then investigated by tensile tests, followed by surface morphology examination using Atomic Force Microscopy (AFM) and Environmental Scanning Electron Microscopy (ESEM). An interdisciplinary approach was applied for establishing a relation between POSS–PI composites chemical microstructure properties and failure mechanisms. Inter molecular POSS–POSS interaction by either phase separation, or chemical POSS–POSS condensation reaction were observed as key factors, affecting the nanocomposite mechanical properties via formation of aggregates. The amount and density of these aggregates were shown to be composition dependent. A model based on formation and coalescence of voids during tensile tests was suggested for understanding the effect of the POSS content on the POSS–PI mechanical response.

1. Introduction

Nowadays, numerous satellites are being launched into low Earth orbit (LEO) altitudes, ranging from 200 to 800 km. The degrading environment in LEO includes atomic oxygen (AO), ultraviolet (UV) and ionizing radiation, ultrahigh vacuum (UHV), thermal cycling, and ultrahigh velocity micrometeoroids and orbital debris [1–3]. The breakup of satellites, either deliberately or accidentally, leads to an increasing amount of orbital debris, which further leads to additional events of ultrahigh velocity impacts onto satellites' external surfaces. Polyimides (PIs) such as Kapton® are used extensively in spacecraft external surfaces as thermal blankets, in solar arrays, and space inflatable structures [4,5] due to their outstanding thermal stability and mechanical properties [6]. PI surfaces coated with SiO_2 have been shown to exhibit AO erosion resistance; however, inherent or hypervelocity debris-induced defects in the coating will permit AO penetration and attack of the underlying polymer [7]. Developing materials which can sustain such impacts and still function under the harsh conditions of the LEO environment is therefore needed. In the past two decades, polymer nanocomposites have attracted a great deal of research attention because, if well dispersed, they may exhibit substantially improved physical and mechanical properties. Polymer based nanocomposites are a novel class of materials that are reinforced by one or more types of fillers of which at least one dimension of the dispersed particles in the polymer matrix is in the nanometer range [8].

A promising approach toward the production of LEO survivable polymer based nanocomposite is incorporation of inorganic Polyhedral Oligomeric Silsesquioxane (POSS) into the organic polymeric chains [9–11]. POSS-containing PIs have shown significantly lower AO erosion yields than pure PI, since AO irradiation results in formation of SiO_2 passivation layer, which protects the underlying polymer from further AO attack [9].

In previous studies, PI and POSS–PI nanocomposite films were exposed to hypervelocity impacts and subsequent air RF plasma (which simulates AO exposure) [7]. Due to this exposure, an impacted PI film eroded one order of magnitude faster than impacted 15 wt.% POSS–PI. The accelerated erosion of the PI is characterized mainly by the formation of RF plasma-induced new macro-holes. A model was suggested to explain this phenomenon, based on the formation of residual tensile stresses around the impacted area. These residual stresses are formed due to the instantaneous loading and elevated temperatures that developed at the time of ultrahigh velocity impact. The residual stresses generate a local increase in the polymer free volume, which facilitates oxygen diffusion into the polymer, thus initiating the process of local high-rate erosion [5,7,12,13]. The low erosion rate of the impacted 15 wt.% POSS–PI film was attributed to both mechanical (i.e. no residual tensile stresses) and chemical (i.e. formation of an oxide passivation layer) aspects [7].

* Corresponding author. Address: Space Environment Section, Soreq NRC, Yavne 81800, Israel. Tel.: +972 8 943 4397; fax: +972 8 943 4403.
E-mail address: rverker@soreq.gov.il (R. Verker).

0266-3538/$ - see front matter © 2009 Elsevier Ltd. All rights reserved.
doi:10.1016/j.compscitech.2009.06.001

The different response of PI and POSS–PI to ultrahigh velocity impacts and AO exposure [7] have initiated a fundamental study of both mechanical properties and chemical composition of these materials. In the present work the chemical analysis of POSS–PI polymerization and surface morphology studies are used to explain the effect of the POSS content on the mechanical properties and the fracture mechanism.

2. Experimental

POSS–PI samples were prepared from blends of oxydianiline–pyromellitic dianhydryde (ODA–PMDA) polyimide (Pyre-M.L. RC-5019 by Industrial Summit Technology, Co.) and TriSilanolPhenyl (TSP)–POSS (Hybrid Plastics, Inc.). Samples were produced in the form of thin films, with different POSS contents of 0 (pure PI), 5, 10 and 15 wt.%.

Films for tensile tests were produced by casting a pre-mixed solution of polyamic acid and POSS in N-methyl-pyrrolidone (NMP) solvent into a glass mold. Samples for Fourier Transform Infrared (FTIR) spectroscopy measurements of POSS–PI were produced by spin coating of the pre-mixed solution on Germanium discs. Two drops of pre-mixed solution were deposited on each disc. The disc was accelerated to 6000 rpm in 30 s and dwelled at 6000 rpm for 60 s, until the film was sufficiently thin to be within the absorbance range where the Beer–Lambert law is obeyed. The curing of the pre-mixed solution is based on a process developed by DuPont, Inc. and described elsewhere [7]. TSP–POSS sample for FTIR measurement was prepared from a solution of 330 mg TSP–POSS dissolved in 6 mL NMP. One drop of the solution was deposited on a Germanium disc, and the NMP was evaporated under vacuum conditions at RT overnight.

Mechanical properties of 25–30 μm thick POSS–PI free standing films were measured according to the specifications of ASTM D882-88, at a strain rate of 20 mm/min. Specimens having a constant width of 3.5 mm in the gauge region were die-cut into dog-bone shape samples. The initial distance between grips was 43 mm. Tests were performed using a universal testing machine (Instron model 1026) equipped with a load cell of 2 kg. Five samples of each POSS–PI composition were tensile tested.

FTIR spectra were obtained using Bruker Vertex 70 spectrometer. At least of 32 scans at a resolution of 4 cm^{-1} were performed for each sample.

The surface morphology of the samples was studied using an Atomic Force Microscope (AFM, Nanoscope IV MultiMode from Veeco). Image analysis of the AFM results was performed using the WSxM software package by Nanotec Electronica [14]. Environmental Scanning Electron Microscopy (ESEM) images of the tensile tested fracture surfaces were obtained using a Quanta 200 microscope by FEI.

3. Results and discussion

Typical tensile stress–strain curves of POSS–PI nanocomposites and the parent PI are shown in Fig. 1. These tests show a ductile-to-brittle transition, with a maximum elongation and tensile strength at 5 wt.% POSS. The tensile tests were performed at room temperature. The PI sample (Fig. 1, curve A), exhibits a gradual transition from elastic to plastic behavior, without a well-defined yield point. A similar behavior is observed for the POSS–PI samples (Fig. 1, curves B, C and D). Addition of 5 wt.% POSS to the PI matrix improves its toughness in comparison to pure PI. The tensile strength and elongation at break of the 5 wt.% POSS–PI sample are 154 MPa and 42%, respectively. The tensile strength and elongation at break of the pure PI are 138 MPa and 31%, respectively. Increase in the POSS content to 10 wt.% POSS leads to reduction in toughness compared to PI. The tensile strength and elongation at break of the 10 wt.% POSS–PI are 118 MPa and 17%, respectively. Further increase in POSS content up to 15 wt.% POSS leads to further reduction in toughness, resulting in the lowest tensile strength and elongation at break of 104 MPa and 12%, respectively. The reduction in toughness of the 10 and 15 wt.% POSS-containing PI may be an indication of disruption of the polymer molecular structure [15], which does not occur with the 5 wt.% POSS–PI. The increase in the 5 wt.% POSS–PI toughness is an indication of an interaction between the PI chains and the POSS at that composition. This interaction may be associated with either crazing [16,17] or chemical cross-linking, as will be further discussed.

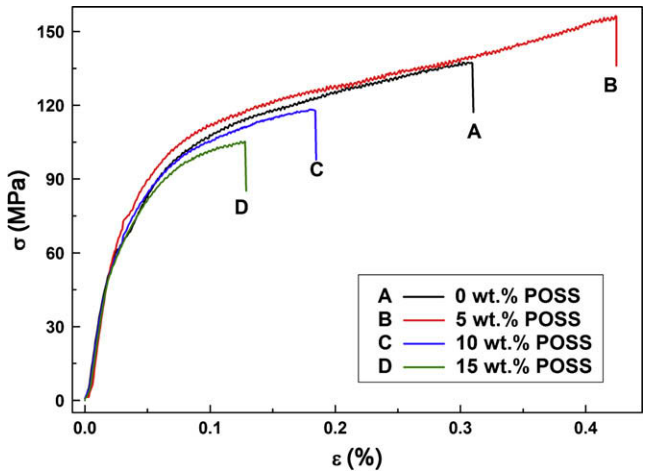

Fig. 1. Typical stress–strain curves at room temperature of POSS–PI films containing 0, 5, 10 and 15 wt.% POSS.

In order to understand the differences in mechanical properties between POSS–PI samples and PI in terms of chemical bonding, the curing process of PI and 15 wt.% POSS–PI was monitored using FTIR spectroscopy. FTIR spectroscopy was used to follow reactions between POSS silanol groups and polyamic acid functional groups, as well as silanol–silanol condensation reactions [18]. Scheme 1a shows the molecular structure of polyamic acid formed by condensation polymerization of oxydianiline (ODA) and pyromellitic dianhydryde (PMDA). Imidization through curing of the polyamic acid leads to the formation of PMDA–ODA PI, as shown in Scheme 1b [19]. Scheme 1c shows the TSP–POSS molecule [15].

POSS molecules containing silanol groups can react, creating either linked POSS molecules by a bridging oxygen atom via silanol–silanol condensation, or physical aggregation via phase separation. Physical aggregation may occur due to decrease in miscibility of the polymer precursor as its molecular weight is gradually increased through curing [20]. POSS molecules may also react with a polymeric matrix, forming a network [21–24].

Fig. 2a shows FTIR spectra of PI and 15 wt.% POSS–PI samples after curing. The main peaks, which appear in both spectra, are the imide carbonyl C=O stretching vibration at 1725 cm^{-1}, aromatic ring stretching vibration at 1498 cm^{-1}, imide ring C–N stretching vibration at 1380 cm^{-1}, and aromatic ether C–O stretching vibration at 1245 cm^{-1} [25]. Fig. 2b shows the Si–O–Si stretching vibration region from 1200 to 1020 cm^{-1} of PI, 15 wt.% POSS–PI and pure TSP–POSS, which serves as a reference. The high resolution FTIR spectra of Fig. 2b emphasize the differences between PI and 15 wt.% POSS–PI. The 15 wt.% POSS–PI spectrum shows two peaks at 1134 cm^{-1} and at 1058 cm^{-1} which are not apparent in the PI FTIR spectrum. The peak at 1134 cm^{-1} belongs to Si–O–Si cage stretching vibration. The peak at 1058 cm^{-1} is attributed to Si–O–Si network stretching vibration [26]. The FTIR reference spectrum of TSP–POSS shows a large peak at 1134 cm^{-1}, which belongs

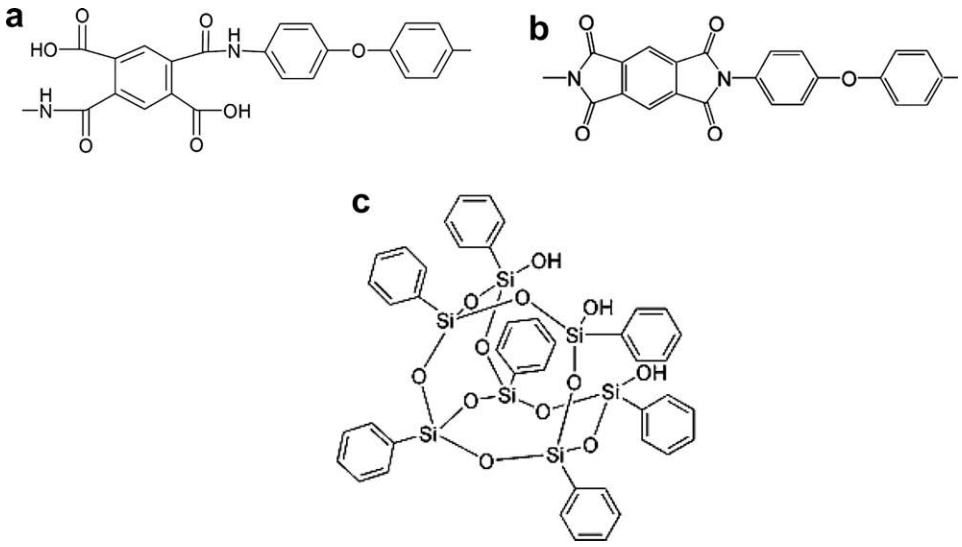

Scheme 1. Schematic presentation of polyamic acid (a), PMDA–ODA PI monomer (b) and TSP–POSS molecule (c).

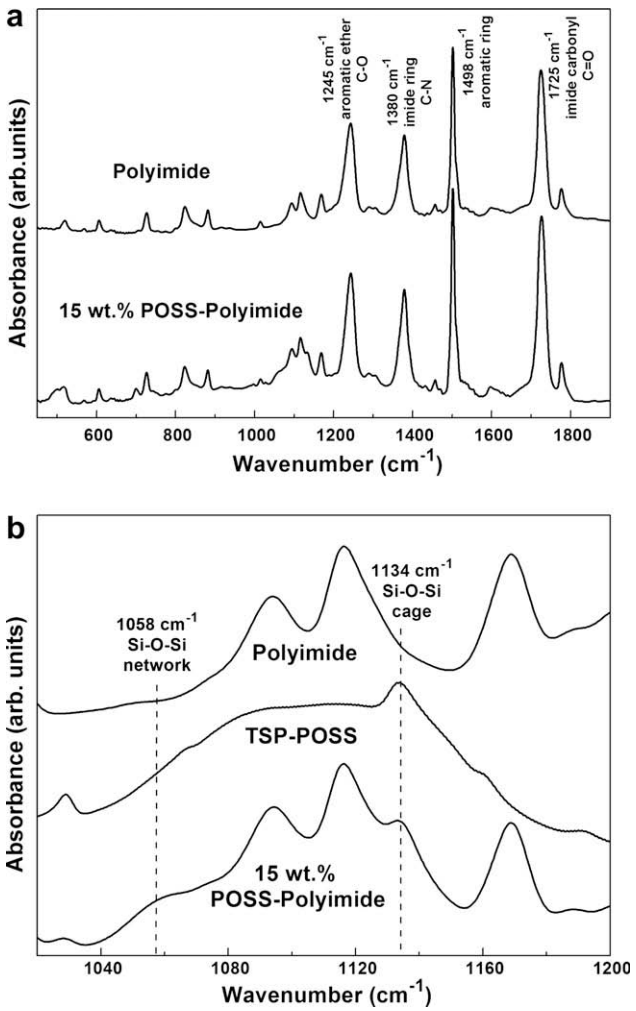

Fig. 2. FTIR spectra of pristine PI, TSP–POSS and 15 wt.% POSS–PI films: (a) wide range scan of PI and 15 wt.% POSS–PI, (b) zoom-in on the Si–O–Si stretching vibration region that includes also TSP–POSS reference spectrum.

to Si–O–Si cage stretching vibration. The peak at 1058 cm^{-1} (Fig. 2b) is an indication of a network of Si–O–Si groups, which are the result of POSS–POSS reaction via condensation. The Si–O–Si networking groups appear only in the 15 wt.% POSS–PI spectrum, which was exposed to a curing temperature of 350 °C, and not in the TSP–POSS reference spectrum, which was prepared at RT. It is a clear indication that Si–O–Si networking occurs due to the elevated temperature to which TSP–POSS was exposed during the 15 wt.% POSS–PI curing process.

Fully cured 15 wt.% POSS–PI FTIR spectra did not show formation of covalent bonds between the POSS molecules and the PI matrix, in the framework of the sensitivity of these measurements.

The chemical reactions that may take place during the curing process can be assessed by studying the imidization kinetics of both samples. If silanol groups go through substantial reaction with either amide or carboxylic groups of the polyamic acid, imidization kinetics of POSS–PI will differ from that of PI. Fig. 3 shows the imidization kinetics of PI and 15 wt.% POSS–PI samples. Also shown is the curing temperature vs. curing time.

In order to study the imidization kinetics, a peak height method was used. The aromatic ether C–O stretching vibration was chosen as internal standard while the imide carbonyl C=O stretching vibration was used as the main imide peak for degree of imidization calculation. The degree of imidization was calculated by:

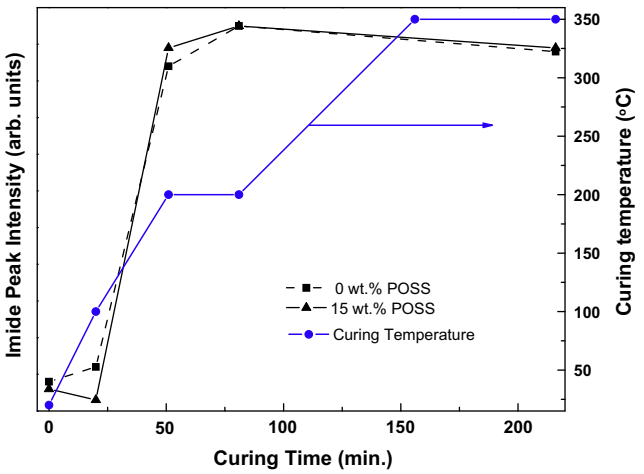

Fig. 3. Imidization kinetics and curing temperature of pure PI and 15 wt.% POSS–PI vs. curing time. Data based on the relative peak intensity of the imide carbonyl stretching vibration at 1725 cm^{-1}.

$$I = \frac{D_{1725\,\mathrm{cm}^{-1}}}{D_{1245\,\mathrm{cm}^{-1}}} \quad (1)$$

where I represents the degree of imidization and D_x is the peak height of the internal standard ($D_{1245\,\mathrm{cm}^{-1}}$) and the imide peak ($D_{1725\,\mathrm{cm}^{-1}}$). The imidization kinetics of the two samples follows a classical pattern [25,27] and shows no major differences. This excludes the possibility of a major chemical reaction in which amid or carboxylic groups from the polyamic acid being consumed by silanol groups of the POSS molecules and the formation of covalent bonds between POSS and PI chains. However, the existence of minor reactions between silanol and amid or carboxylic groups, which are beyond the sensitivity of the FTIR measurements, still have to be taken into consideration. Such minor reactions may not affect the reaction kinetics, but may affect on the resultant structure and properties.

Fig. 3 shows a small reduction in imide peak height of both samples from a curing temperature of 200 °C to the final curing temperature of 350 °C. This reduction may be attributed to a change in configuration of the imide ring, which causes a change in the carbonyl symmetric stretch dipole [28].

POSS–POSS reaction mechanism via Si–O–Si networking or via physical aggregation is further supported by POSS–PI surface morphology obtained using AFM. Fig. 4 shows AFM images of pristine PI film (a), 5 (b), 10 (c) and 15 (d) wt.% POSS–PI films. The surface morphology of the PI sample is smooth, except for some scratches apparent on the surface. The POSS–PI samples reveal rather different morphology, which is characterized mainly by the appearance of aggregates on the surface. Increase of the POSS content resulted in an apparent increase in the aggregates size and density. Image analysis of the AFM data was used to quantify the aggregates average diameter d_a, the inter-aggregate distance τ, and the surface density ρ_s. The results are summarized in Table 1.

As shown in Table 1, higher POSS content ($\geqslant$10 wt.%) results in higher aggregates average diameter and in a somewhat lower inter-aggregate distance. The average aggregates surface density attain a maximum at 10 wt.% POSS, while at 5 and 15 wt.% POSS content the aggregates surface density is lower. Fig. 5 shows the total interface length L between POSS aggregates and PI matrix vs. POSS content. The total interface length was calculated according to:

$$L = \pi \cdot d_a \cdot \rho_s \quad (2)$$

Fig. 5 also shows the toughness U_T of the POSS–PI samples vs. POSS content, as derived from the tensile test results shown in Fig. 1. The toughness was calculated by:

$$U_T = \int_0^{\varepsilon_b} \sigma \cdot \mathrm{d}\varepsilon \quad (3)$$

where σ is the tensile stress, ε is the strain and ε_b is the strain at break. The results of Fig. 5 demonstrate a correlation between the mechanical properties of POSS–PI and its morphology at the nano level. While the total POSS–PI interface length of the 5 wt.% POSS–PI is the lowest, its toughness is the highest. The results for the 10 and 15 wt.% POSS–PI samples represent a tradeoff between the aggregates diameter and density. The 10 wt.% POSS–PI aggregates are much smaller compared to the 15 wt.% POSS–PI aggregates.

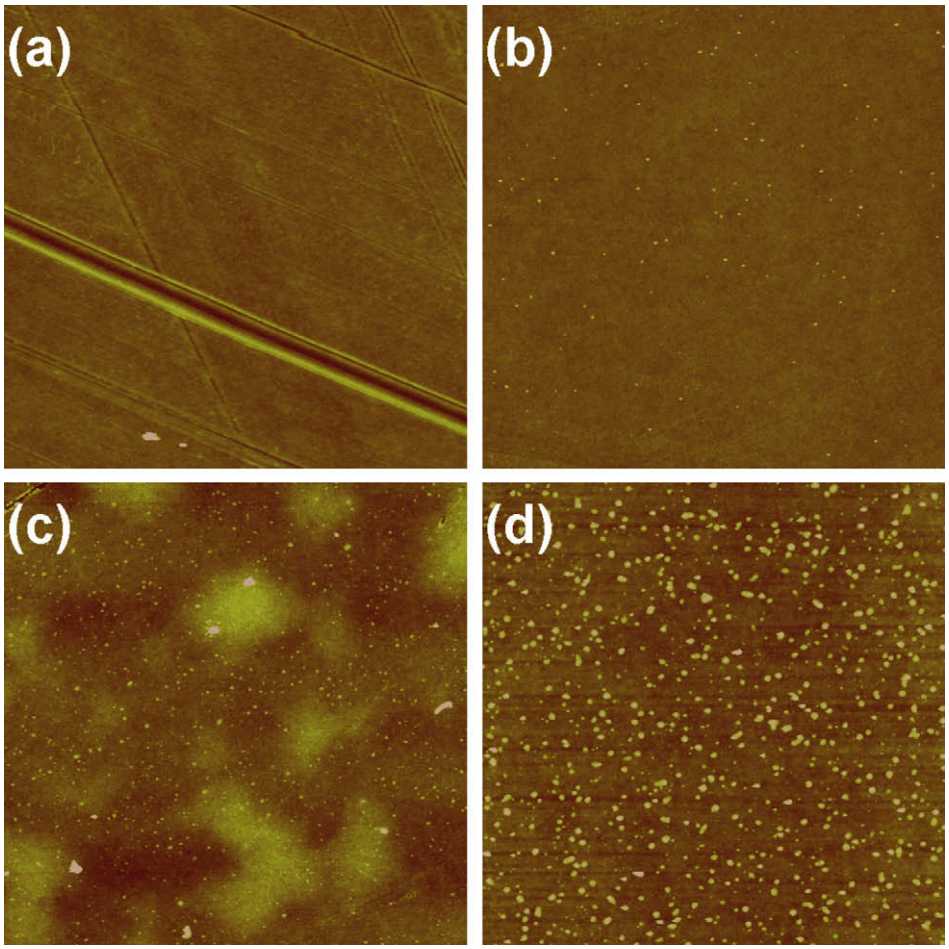

Fig. 4. AFM images of pristine PI (a), and 5 (b), 10 (c) and 15 (d) wt.% POSS–PI films. Scan size: 5 × 5 μm, z-range: 25 nm.

Table 1
Aggregates average diameter d_a, inter-aggregate distance τ, and surface density ρ_s, obtained by image analysis of Fig. 4.

Aggregate parameter	POSS (wt.%)		
	5	10	15
d_a (nm)	26	28	47
τ (nm)	200	87	103
ρ_s (#/μm^2)	4	72	36

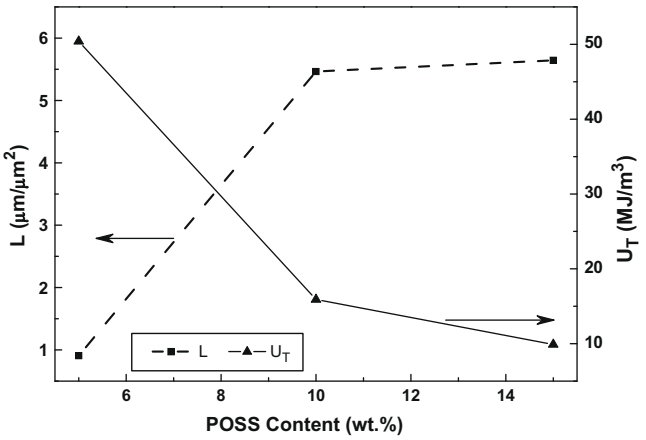

Fig. 5. The average POSS–PI interface length L and toughness U_T as a function of the POSS content, exhibiting an inverse dependence.

On the other hand, the surface density of the 10 wt.% POSS–PI aggregates is higher compared to the 15 wt.% POSS–PI aggregates surface density. The total interface length of both of these samples is almost similar, and so is their toughness. Ojeda and Martin [19] have shown that the morphology of PMDA–ODA PI consists of spherulitic bundles of well-defined lamellae similar to that typically observed in semicrystalline polymers. The lamellar crystal thickness was found to be 5–15 nm, corresponding to six PMDA–ODA repeat units along the chain axis [19]. The effect of the aggregates density and size on the mechanical properties of the nanocomposites was also studied in various organic–inorganic nanocomposite systems. For example, it was found that the yield stress of silica fillers embedded in polyamide 6 is sensitive to the volume fraction, and also to the filler size and dispersion state. This may indicate the existence of an optimal size for the reinforcing particles [16,29]. In the case of POSS–PI nanocomposites, the aggregate diameter depends on POSS content. At low POSS content, as in the case of 5 wt.% POSS–PI, the aggregates diameter and the PI lamella thickness are close in size, while the inter-aggregate distance is large, resulting in toughness improvement. However, at higher POSS content, as in the case of 15 wt.% POSS–PI, when the aggregates diameter exceeds the PI's lamella thickness by a factor of four, and the inter-aggregate distance is low, toughness deteriorates. Based on existing theories [29,30], the effect of the aggregates' diameter, density and inter-aggregate distance on the mechanical properties can be defined. While applying load, e.g. during tensile test, the POSS aggregates debond from the PI matrix, leading to the formation of voids around the aggregates as the polymer is plastically deformed. At low POSS content, such as in 5 wt.% POSS–PI, which is characterized by small aggregates' diameter, a large inter-aggregate distance and low surface density, lateral coalescence of the voids is avoided while the width of the ligaments between the aggregates decreases with elongation. Each void serves independently in allowing higher degree of elongation compared to PI, leading to higher toughness, as shown schematically in Fig. 6a. Fractography of a 5 wt.% POSS–PI sample is shown in Fig. 6c. The addition of 5 wt.% POSS did not affect the fracture mode, which was similar to that of pure PI film (not shown). The fracture initiated at the edge of the sample gauge section, propagating by a fast brittle cracking mechanism. At higher POSS content, such as in 15 wt.% POSS–PI, the POSS aggregates also debond, and voids are formed. However, the small inter-aggregate distance and large aggregates' diameter and surface density, compared to 5 wt.% POSS–PI, lead to lateral coalescence of the voids at early stages of the tensile test. This process is accompanied by high local stress acting on the thin ligaments between the aggregates. The lateral coalescence of the voids reduced the sample ability to withstand the stress loads, as shown in Fig. 6b. When the thin ligaments could not support anymore the load, they fractured. Coalescence into critical-sized voids could occur at any location along the gauge section. At the critical-size void sites, the polymer failed through ductile tearing followed by faster brittle cracking of the rest of the sample. Fig. 6d demonstrates this effect, indicating on a fracture which started near the center of the sample.

To demonstrate the above failure mechanism, the fracture of tensile tested 10 wt.% POSS–PI film was analyzed by AFM. Fig. 7 shows an AFM image of the fractured surface which reveals the structure after the tensile test. The fractured surface is characterized by aggregates, 30–40 nm in diameter, embedded in voids. According to the suggested failure mechanism, fracture will occur after debonding of the aggregates from the matrix and coalescence of the created voids. The image demonstrates clearly the debonding phenomenon and the voids formation. Also seen on the upper left-hand side of the image two pairs of aggregates embedded in a single void. Each of these single voids possibly originated from coalescence of two voids during the tensile test.

The densities of POSS and PI are 1.12 and 1.42 g cm^{-3}, respectively [31,32]. Accordingly, the theoretical volume content (POSS vol.%) of the 5, 10 and 15 wt.% POSS–PI is 6, 12 and 18 vol.%, respectively. Based on the AFM images of Fig. 4, the POSS volume percent $V_{\%}$ was estimated to be:

$$V_{\%} = \frac{\rho_s \cdot V_a \cdot l_s}{V_T} \cdot 100 \tag{4}$$

$$l_s = \frac{\sqrt[3]{V_T}}{d_a} \tag{5}$$

where V_a is the average single aggregate volume and l_s is the number of layers which form V_T, the total nanocomposite volume. The above calculation is based on the assumption that the aggregates diameter and inter-aggregate distance on the surface represent also the bulk aggregates. Using Eq. (4), the POSS–PI aggregates volume content for the 5, 10 and 15 wt.% is estimated as 0.05, 0.6 and 1.3 vol.%, respectively. The results show that only a small fraction of the incorporated POSS appears as POSS aggregates. It is thus assumed that the rest of the incorporated POSS molecules are dissolved in the PI matrix as molecules, olygomers or as very small aggregates (<10 nm). Scheme 2 is an attempt to represent the POSS–PI structure based on the obtained chemical, mechanical and morphological data.

The POSS–PI nanocomposite morphology is based on the semicrystalline PI matrix and POSS molecules. The PI chains appear either in lamellar structure or as an unordered amorphous phase [19]. Most of the POSS molecules are dispersed in the PI matrix as very small aggregates (<10 nm) comprised of few molecules or as single molecules. However, a little amount of POSS molecules forms large aggregates, 20 nm or larger. The diameter and inter-aggregate distance of these aggregates have a significant impact on the POSS–PI mechanical properties, as explained before by the fracture model.

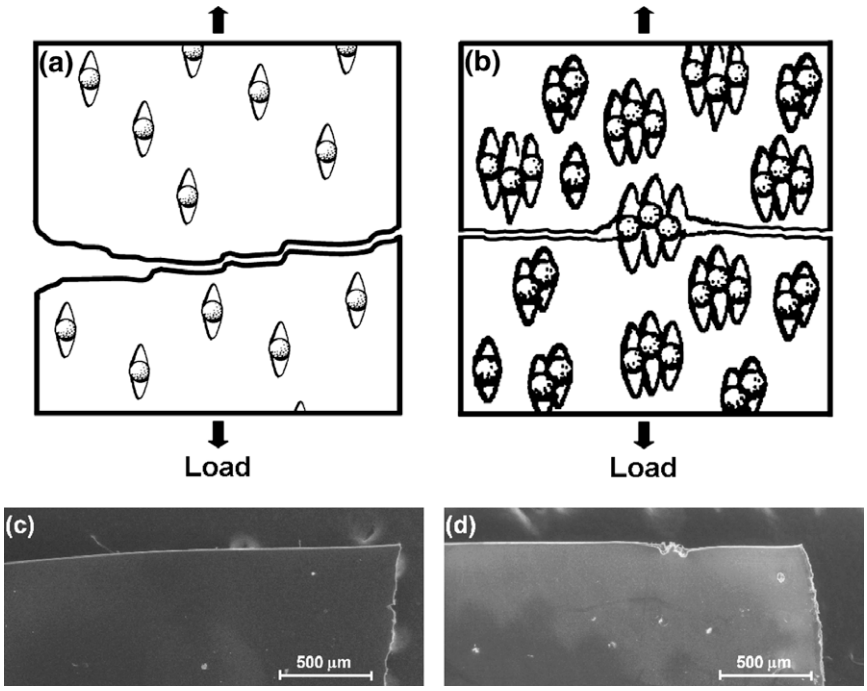

Fig. 6. Schematic presentation of the fracture mode of POSS–PI films with low (a) and high (b) POSS content (adopted from Ref. [30]). ESEM images of the fracture surfaces of tensile tested 5 wt.% (c) and 15 wt.% (d) POSS–PI films, demonstrating the suggested fracture modes in (a) and (b), respectively. Note the origin of the fracture at the center of the high POSS content sample (d).

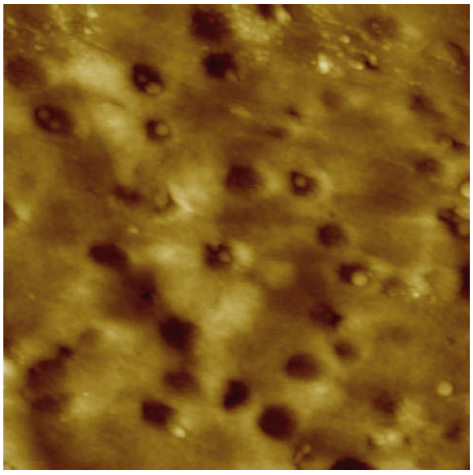

Fig. 7. AFM image of the fracture surface of a tensile tested 10 wt.% POSS–PI film. Scan size: 2 × 2 μm, *z*-range: 85 nm.

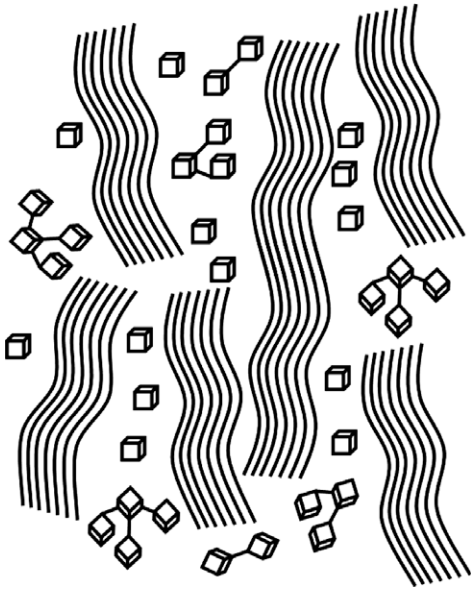

Scheme 2. Schematic presentation of the POSS–PI nanocomposite, showing the PI lamella structure, POSS aggregates and POSS single molecules.

4. Conclusions

The mechanical properties and fracture mechanism of POSS–PI nanocomposites were shown to be dependent on the amount of POSS content. Imidization kinetics and FTIR spectroscopy indicate on no major chemical reaction taking place between the POSS molecules and the PI chains. It was found that most of the POSS incorporated in the PI matrix was dissolved as single molecules or as small aggregates (<10 nm).

AFM study revealed the formation of POSS aggregates, and showed that the aggregates diameter, inter-aggregate distance and surface density depend on the POSS content. A correlation between the aggregates parameters and the mechanical properties of the nanocomposite was established.

A model demonstrating the effect of the POSS content on the POSS–PI mechanical properties was suggested. This model is based on voids formation around the aggregates during tensile loading and coalescence of the voids if their diameter, distance and density are above a critical value. Fractography results support the suggested aggregates-based model, showing different fracture modes as a function of the POSS content.

References

[1] Bedingfield KL, Leach RD, Alexander MB. NASA Reference Publication 1390; 1996.
[2] Tribble AC. The space environment: implementation for spacecraft design. Princeton (NJ): Princeton University Press; 1995.
[3] Grossman E, Gouzman I. Nucl Instrum Methods Phys Res Sect B – Beam Interact Mater Atoms 2003;208:48–57.
[4] Connell JW, Watson KA. High Perform Polym 2001;13(1):23.
[5] Verker R, Grossman E, Gouzman I, Eliaz N. Polymer 2007;48(1):19.
[6] Musto P, Ragosta G, Scarinzi G, Mascia L. Polymer 2004;45(12):4265.
[7] Verker R, Grossman E, Gouzman I, Eliaz N. High Perform Polym 2008;20(4–5):475–91.
[8] Boo WJ, Liu J, Sue HJ. Mater Sci Technol 2006;22(7):829–34.
[9] Brunsvold AL, Minton TK, Gouzman I, Grossman E, Gonzalez R. High Perform Polym 2004;16(2):303–18.
[10] Gilman JW, Schlitzer DS, Lichtenhan JD. J Appl Polym Sci 1996;60(4):591.
[11] Gonzalez RI. PhD thesis, Department of Chemical Engineering, University of Florida, Gainesville, Florida; 2002.
[12] Verker R, Eliaz N, Gouzman I, Eliezer S, Fraenkel M, Maman S, et al. Acta Mater 2004;52(19):5539.
[13] Tyler DR. J Macromol Sci – Polym Rev 2004;C44(4):351–88.
[14] Horcas I, Fernandez R, Gomez-Rodriguez JM, Colchero J, Gomez-Herrero J, Baro AM. Rev Sci Instrum 2007;78(1).
[15] Zhao YQ, Schiraldi DA. Polymer 2005;46(25):11640–7.
[16] Jordan J, Jacob KI, Tannenbaum R, Sharaf MA, Jasiuk I. Mater Sci Eng A – Struct Mater Properties Microstruct Process 2005;393(1–2):1–11.
[17] Ash BJ, Rogers DF, Wiegand CJ, Schadler LS, Siegel RW, Benicewicz BC, et al. Polym Compos 2002;23(6):1014–25.
[18] Xie B, Muscat AJ. IEEE Trans Semiconduct Manufact 2004;17(4):544–53.
[19] Ojeda JR, Martin DC. Macromolecules 1993;26(24):6557–65.
[20] Amici M. PhD thesis. Ecole Doctorale Materiaux de Lyon; 2006.
[21] Dijkstra TW, Duchateau R, van Santen RA, Meetsma A, Yap GPA. J Am Chem Soc 2002;124(33):9856–64.
[22] Liu YR, Huang YD, Liu L. Compos Sci Technol 2007;67(13):2864–76.
[23] Liang KW, Li GZ, Toghiani H, Koo JH, Pittman CU. Chem Mater 2006;18(2):301–12.
[24] Morrison JJ, Love CJ, Manson BW, Shannon IJ, Morris RE. J Mater Chem 2002;12(11):3208–12.
[25] Hsu TCJ, Liu ZL. J Appl Polym Sci 1992;46(10):1821–33.
[26] Eon D, Raballand V, Cartry G, Cardinaud C, Vourdas N, Argitis P, et al. J Vac Sci Technol B 2006;24(6):2678–88.
[27] Nishino T, Kotera M, Inayoshi N, Miki N, Nakamae K. Polymer 2000;41(18):6913–8.
[28] Snyder RW, Sheen CW, Painter PC. Appl Spectrosc 1988;42(3):503–8.
[29] Reynaud E, Jouen T, Gauthier C, Vigier G, Varlet J. Polymer 2001;42(21):8759–68.
[30] Li JX, Hiltner A, Baer E. J Appl Polym Sci 1994;52(2):269–83.
[31] Leu CM, Chang YT, Wei KH. Chem Mater 2003;15(19):3721–7.
[32] Leu CM, Reddy GM, Wei KH, Shu CF. Chem Mater 2003;15(11):2261–5.